Atmos. Meas. Tech., 17, 5413–5428, 2024 https://doi.org/10.5194/amt-17-5413-2024 © Author(s) 2024. This work is distributed under the Creative Commons Attribution 4.0 License.





Ammonium CI-Orbitrap: a tool for characterizing the reactivity of oxygenated organic molecules

Dandan Li¹, Dongyu Wang², Lucia Caudillo³, Wiebke Scholz⁴, Mingyi Wang^{5,a}, Sophie Tomaz¹, Guillaume Marie³, Mihnea Surdu², Elias Eccli⁴, Xianda Gong⁶, Loic Gonzalez-Carracedo⁷, Manuel Granzin³, Joschka Pfeifer^{3,8}, Birte Rörup⁹, Benjamin Schulze^a, Pekka Rantala⁹, Sébastien Perrier¹, Armin Hansel⁴, Joachim Curtius³, Jasper Kirkby^{3,8}, Neil M. Donahue⁵, Christian George¹, Imad El-Haddad², and Matthieu Riva¹

University of Helsinki, 00014 Helsinki, Finland

Correspondence: Matthieu Riva (matthieu.riva@ircelyon.univ-lyon1.fr)

Received: 16 July 2023 – Discussion started: 15 August 2023

Revised: 16 May 2024 - Accepted: 17 May 2024 - Published: 13 September 2024

Abstract. Oxygenated organic molecules (OOMs) play an important role in the formation of atmospheric aerosols. Due to various analytical challenges with respect to measuring organic vapors, uncertainties remain regarding the formation and fate of OOMs. The chemical ionization Orbitrap (CI-Orbitrap) mass spectrometer has recently been shown to be a powerful technique that is able to accurately identify gaseous organic compounds due to its greater mass resolution. Here, we present the ammonium-ion-based CI-Orbitrap (NH₄⁺-Orbitrap) as a technique capable of measuring a wide range of gaseous OOMs. The performance of the NH₄⁺-Orbitrap is compared with that of state-of-the-art mass spectrometers, including a nitrate-ion-based chemical ionization atmospheric pressure interface coupled to a time-of-flight mass spectrometer (NO₃-LTOF), a new generation of proton transfer reaction-TOF mass spectrometer (PTR3-TOF), and an iodide-based CI-TOF mass spectrometer equipped with a Filter Inlet for Gases and AEROsols (I--CIMS). The instruments were deployed simultaneously in the Cosmic Leaving OUtdoors Droplets (CLOUD) chamber at the European Organization for Nuclear Research (CERN) during the CLOUD14 campaign in 2019. Products generated from α -pinene ozonolysis under various experimental conditions were simultaneously measured by the mass spectrometers. The NH₄⁺-Orbitrap was able to identify the widest range of OOMs (i.e., $O \ge 2$), from less-oxidized species to highly oxygenated organic molecules (HOMs). Excellent agreement was found between the NH_4^+ -Orbitrap and the NO_3^- -LTOF with respect to characterizing HOMs and with the PTR3-TOF for the less-oxidized monomeric species. OOM concentrations measured by NH₄⁺-Orbitrap were estimated using calibration factors derived from the OOMs with high timeseries correlations during the side-by-side measurements. As with the other mass spectrometry techniques used during this campaign, the detection sensitivity of the NH₄⁺-Orbitrap to OOMs is greatly affected by relative humidity, which may be related to changes in ionization efficiency and/or multiphase chemistry. Overall, this study shows that NH₄⁺-ionbased chemistry associated with the high mass resolution of the Orbitrap mass analyzer can measure almost all inclusive

¹Universite Claude Bernard Lyon 1, CNRS, IRCELYON, UMR 5256, 69100 Villeurbanne, France

²Laboratory of Atmospheric Chemistry, Paul Scherrer Institute, 5232 Villigen, Switzerland

³Institute for Atmospheric and Environmental Sciences, Goethe University Frankfurt, 60438 Frankfurt am Main, Germany

⁴Institute for Ion Physics and Applied Physics, University of Innsbruck, 6020 Innsbruck, Austria

⁵Center for Atmospheric Particle Studies, Carnegie Mellon University, Pittsburgh, PA 15213, USA

⁶Department of Atmospheric Microphysics, Leibniz Institute for Tropospheric Research, 04318 Leipzig, Germany

⁷Faculty of Physics, University of Vienna, 1090 Vienna, Austria

⁸CERN, the European Organization for Nuclear Research, 1211 Geneva 23, Switzerland

⁹Institute for Atmospheric and Earth System Research/Physics, Faculty of Science,

anow at: Department of the Geophysical Sciences, University of Chicago, Chicago, IL 60637, USA

compounds. As a result, it is now possible to cover the entire range of compounds, which can lead to a better understanding of the oxidation processes.

1 Introduction

Aerosols affect the climate by directly scattering or absorbing solar radiation or by acting as seeds for cloud formation (Fan et al., 2016; Haywood and Boucher, 2000). A major fraction of submicron aerosol mass consists of organic compounds, with secondary organic aerosol (SOA) predominating (Jimenez et al., 2009; Hallquist et al., 2009). Oxygenated organic molecules (OOMs) generated from the oxidation of volatile organic compounds (VOCs) contribute to the formation and growth of SOA (Ehn et al., 2014; Mellouki et al., 2015). OOMs can be generated via the bimolecular peroxy radicals (RO₂) pathway or by the autoxidation of RO₂ followed by the termination pathways (Bianchi et al., 2019; Mohr et al., 2019). Among OOMs, highly oxygenated organic molecules (HOMs), containing multiple functional groups and exhibiting (extremely) low saturation vapor pressure, can nucleate in concert with inorganic species, for example, with sulfuric acid or on their own (Ehn et al., 2014; Kirkby et al., 2016; Bianchi et al., 2016), forming new particles. Less-oxygenated molecules (i.e., containing two to five oxygen atoms) play a vital role in the growth of newly formed atmospheric particles, either by condensation or through multiphase chemistry (Bianchi et al., 2019; Ehn et al., 2014; Hallquist et al., 2009). Therefore, the identification and quantification of the wide diversity of OOMs are essential to understand SOA formation and growth (Kirkby et al., 2016; Bianchi et al., 2016; Ehn et al., 2014).

Mass spectrometry (MS) has resulted in remarkable achievements with respect to the detection, characterization, and quantification of OOMs (Wang et al., 2020; Breitenlechner et al., 2017; Bianchi et al., 2019; Ehn et al., 2010; Riva et al., 2019a). Moreover, the application of chemical ionization (CI) enables the detection of a wide variety of organic and inorganic analytes (Bianchi et al., 2019; Ehn et al., 2014; Jokinen et al., 2012; Lee et al., 2014). However, the selection of ionization chemistry in combination with the MS detection technique will impact the selectivity and sensitivity of the methods toward certain groups of OOMs (Bianchi et al., 2019; Riva et al., 2020, 2019b; Berndt et al., 2018b, a). For example, negative-ion-based chemistry, including nitrate (NO₃⁻), can optimally detect HOMs, which only constitute a small subset of the OOMs (Lee et al., 2014; Berndt et al., 2018b; Riva et al., 2019b); iodide (I⁻) can efficiently detect various OOMs with three to five oxygen atoms (Riva et al., 2019b; Lee et al., 2014). Positive-ion-based chemistries have also been developed, showing great sensitivity to HOMs as well as less-oxidized products, providing the possibility to achieve carbon closure of the OOMs (Berndt et al., 2018a, b; Hansel et al., 2018; Riva et al., 2020, 2019b). However, these positive-ion methods are mainly based on proton transfer and often result in fragmentation of the analytes (Breitenlechner et al., 2017). Time-of-flight (TOF) mass spectrometers using ammonium (NH_4^+) or amines as reagent ions can detect a wide variety of OOMs but suffer from a lack of mass resolution, making peak identification challenging, especially for complex systems, i.e., under ambient conditions (Berndt et al., 2018b, a; Riva et al., 2019b). Finally, the recently developed Orbitrap mass spectrometer using propylamine has achieved unambiguous identification of overlapping peaks and accurate quantification of OOMs (Riva et al., 2020). However, this analytical technique has been used in very diluted and dry environments to ensure a linear response to the OOMs produced from simple atmospheric systems, i.e., a single VOC precursor and oxidant (Riva et al., 2020, 2019b).

Here, we explore the capability of an NH₄⁺-ion-based CI-Orbitrap mass spectrometer (Q Exactive Orbitrap, Thermo Scientific) to detect OOMs generated from α-pinene ozonolysis in the Cosmic Leaving OUtdoors Droplets (CLOUD) chamber at the European Organization for Nuclear Research (CERN) under various environmental conditions. We compare the performance of the NH₄⁺-Orbitrap to state-of-theart online mass spectrometers, including a nitrate CI atmospheric pressure interface long time-of-flight mass spectrometer (NO₃⁻-LTOF; TOFWERK AG), a proton transfer reaction time-of-flight mass spectrometer (PTR3-TOF; ION-ICON Analytik GmbH), and the gas phase of an iodide CI time-of-flight mass spectrometer equipped with a Filter Inlet for Gases and AEROsols (I⁻-CIMS; TOFWERK AG).

2 Experimental approach and product analysis

2.1 CLOUD chamber experiments

All experiments were conducted in the CLOUD chamber, a 26 m³ cylindrical stainless-steel vessel at CERN. The chamber can achieve a pristine background for the study of nucleation (Kirkby et al., 2016). The chamber operated as a continuously stirred tank reactor (CSTR), with mixing driven by two inductively coupled fans at the top and bottom of the chamber. Evaporated liquid nitrogen (N2) and liquid oxygen (O₂) were blended at a ratio of 79:21 to provide ultrapure synthetic air that constantly flushed the chamber. Variable amounts of trace gases, including O_3 , VOCs, NO_x , SO₂, and CO were accurately injected into the chamber via a gas control system and then monitored. Photolysis was driven by various light sources, including Hg-Xe UV lamps and a UV excimer laser. Between experiments, the chamber was cleaned, by irrigating the walls with ultrapure water; heated to 373 K; and flushed with humidified pure air and high ozone, reducing the contaminant (e.g., VOCs) levels to sub-part-per-trillion-by-volume (pptv) values. During the cleaning process, particles were removed using a highvoltage electric field.

The results presented here are from the CLOUD14 campaign performed in autumn 2019. During CLOUD14, the total flow was kept at 250 slpm (standard liters per minute), providing an average residence time of 104 min. α -Pinene was introduced into the chamber by passing a small flow of dry air over a temperature-controlled evaporator containing liquid α -pinene. Ozone was generated by flowing a small fraction of the air through a quartz tube surrounded by UV-C lights (wavelength < 240 nm). Experiments were performed at low temperature (263 \pm 0.1 K). The relative humidity (RH) in the chamber was controlled by flowing a portion of the air through a Nafion® humidifier using ultrapure water (18 M Ω cm; Millipore Corporation). The contents of the chamber were monitored by a wide range of external instruments connected to sampling probes that protruded ~ 1 m into the chamber.

2.2 Product analysis by NH₄⁺-Orbitrap

The chemical composition of closed-shell molecules was determined in real time by means of a CI-Orbitrap sampling from the CLOUD chamber through a 750 mm long, 10 mm inner diameter Teflon tube at a flow rate of 10 slpm. The CI inlet mounted on the Orbitrap was custom-built with minor modifications from the commercial inlet (Riva et al., 2019a). The ion-molecule reaction (IMR) proceeded at atmospheric pressure with a residence time of 200–300 ms. The same operating parameters used in our previous studies (radio frequency, RF, level of 60; automatic gain control of 1×10^6 charges; maximum injection time of 1000 ms; multi-RF ratio of 1.2; and mass resolution of $m/\Delta m$ 140 000 at m/z 200) were used, thereby minimizing declustering and maximizing the linearity range (Riva et al., 2019a, 2020; Cai et al., 2022).

The high-resolution Orbitrap mass spectra data were analyzed using "Orbitool" software (https://orbitrap.catalyse.cnrs.fr, last access: 27 August 2024) with a graphical user interface (GUI) (Cai et al., 2021). The analysis procedures included data averaging, noise determination and reduction, single-peak fitting, mass calibration, assignment of molecular formulas, and export of time series. Signals were averaged over 5 min before determining the noise and performing mass calibration.

Ammonium was utilized in the PTR-MS at a low pressure (Berndt et al., 2018b; Hansel et al., 2018). Here, this ionization technique was used to detect OOMs at atmospheric pressure and was operated in a similar fashion to that in our initial study (Riva et al., 2019a). The NH₃ was added into the ion source by flushing 2 sccm (standard cubic centimeters per minute) of dry air over the headspace of a 1 % liquid ammonia—water mixture (prepared from Milli-Q water and 25 % ammonium hydroxide stock solution; ACS reagent, Sigma-Aldrich). The product molecules ("prod") were softly charged by binding to ammonium (NH₄⁺) ions, forming

prod–NH₄⁺ adduct ions or protonated products prod–H⁺, following either Reaction (R1) or (R2):

$$NH_4^+ + prod \rightarrow prod - NH_4^+,$$
 (R1)

$$NH_4^+ + prod \rightarrow prod - H^+ + NH_3.$$
 (R2)

The $\mathrm{NH_4^+}$ reagent ion cannot be directly detected due to the cutoff of the Orbitrap mass analyzer (i.e., m/Q 50). Hence, normalization of the raw analyte signals is difficult and hinders quantification of OOMs. However, we observed a total of 62 peaks corresponding to amines, including $\mathrm{C_4H_{12}N^+}$ and $\mathrm{C_6H_{14}N^+}$, which are formally ammonia derivatives. To some extent, their signals can be used to correct for changes in $\mathrm{NH_4^+}$ ion chemistry. Among these peaks, 13 were abundant and constant throughout the measurement period (Fig. S1 in the Supplement). As a result, these signals were used as surrogates for the primary reagent ions to normalize the signal intensity of the OOMs (Eq. 1) and to account for the potential variation in the ionization process (Riva et al., 2019b).

$$[OOM]_{nor} = \frac{\left[OOM - NH_4^+\right] + \left[OOM - H^+\right]}{\sum [Amine]}$$
 (1)

Correlation analyses were performed between the NH_4^+ -Orbitrap and the two reference instruments, including the NO_3^- -LTOF and PTR3-TOF (referred to as REF). The Pearson correlation coefficient (R^2) values were determined using the time series during two runs (run 2211 and 2213). This included α -pinene (AP) injection, NO_x or CO injections, and RH variation. As a result, for one compound, 755 data points were recorded and used for the correlation analysis. Although product ions with same molecular formulas might lead to low correlation (see details in Sect. 3.3) and would suggest different species (i.e., isomers, fragment ions, etc.), a few molecules with R^2 values greater than 0.9 (18 for NO_3^- -LTOF, 32 for PTR-TOF, and 5 for I^- -CIMS) were selected and were likely attributed to the same species.

Although no direct calibration has been performed for the NH_{Δ}^{+} -Orbitrap, the OOM concentrations were estimated based on comparisons between the NH₄⁺-Orbitrap and the two reference instruments whose quantification methods have been developed and verified. For the OOMs whose time series had R^2 values greater than 0.9 between the NH₄⁺-Orbitrap and REF, linear regression was conducted for normalized intensities in the NH₄⁺-Orbitrap (dimensionless) and concentrations in the REF (molec.cm⁻³), and the slopes were recorded as their relative sensitivity. The calibration factor $c_{\text{Orbi-REF}}$ was derived from the averaged relative sensitivity of these species ($\sim 2.62 \times 10^8 \, \text{molec.cm}^{-3}$ for the NO_3^- -LTOF and $\sim 4.83 \times 10^8$ molec. cm⁻³ for the PTR3-TOF). Applying the calibration factors to all the OOMs, their concentrations detected by the NH₄⁺-Orbitrap could be calculated as shown in Eq. (2). Additionally, a temperaturedependent sampling-line loss correction factor was applied

(Simon et al., 2020).

$$[OOM]_{Orbi-REF} = c_{Orbi-REF} \times [OOM]_{nor}$$
 (2)

2.3 Product analysis by NO₃-LTOF

Detection of RO₂ radicals and closed-shell products was also performed by the NO₃⁻-LTOF, which has been described elsewhere (Jokinen et al., 2012; Caudillo et al., 2021). Only details relevant for this study are provided here. The NO₃⁻-LTOF used in this study had a mass resolution of $m/\Delta m$ 12 000 and detected OOMs (mass 300–650 Da) as clusters ions with (HNO₃) $_n$ (NO₃⁻) anions, where n=0-2. The limit of detection (LoD) for OOMs is 5×10^4 molec. cm⁻³ (Simon et al., 2020). The primary ions were produced by a corona discharge needle exposed to a sheath gas enriched by HNO₃. Laminar flow diffusional loss was assumed in the 30 cm sampling line. A core-sampling technique was applied, which drew a core flow of 5.1 slpm from the center of a 30 slpm total flow. This setup reduced the sampling loss rate of HOMs to less than 30 % (Simon et al., 2020).

The data were processed using Tofware (version 3.2; Aerodyne Inc., USA) and MATLAB R2019b (MathWorks, Inc., USA). In addition, background signals, mass-dependent transmission efficiency (Heinritzi et al., 2016), and sampling losses (Simon et al., 2020) were determined and corrections were applied. The NO₃-LTOF was directly calibrated using sulfuric acid (H₂SO₄), where the detection efficiency of HOMs was assumed to be similar to H₂SO₄. However, OOMs with less oxygen atoms (O < 6) were prone to a lower detection efficiency compared with H2SO4, leading to an underestimation (Stolzenburg et al., 2018; Ehn et al., 2014). A calibration factor C was determined to be $\sim 4.13 \times 10^{10}$ molec. cm⁻³ during CLOUD14 (Caudillo et al., 2021). The concentration of OOMs was also corrected using a mass-dependent transmission efficiency inferred by depleting the reagent ions with several perfluorinated acids. Assuming that OOMs are lost in sampling lines due to diffusion, the losses of OOMs were corrected with a diffusion coefficient scaling with the molecular mass. More information can be found in former studies (Heinritzi et al., 2016; Stolzenburg et al., 2018; Simon et al., 2020; Caudillo et al., 2021).

2.4 Product analysis by PTR3-TOF

The PTR3-TOF ionizes organic compounds by proton transfer or ligand switching reactions in which protonated water clusters $(H_2O)_nH_3O^+$, where n=1–3, are produced by a corona discharge using humidified nitrogen (Breitenlechner et al., 2017). To reduce sample losses, 2 slpm was drawn from a 10 slpm laminar flow through a critical orifice into the tripole where the ion–molecule reactions occur. The pressure in this region was maintained at \sim 80 mbar. The distribution of primary ions and sample molecules can be adjusted by a tunable radio frequency signal applied to the tripole

rods. The LoD of the PTR3-TOF for detecting OOMs is 8×10^5 molec. cm⁻³ (Breitenlechner et al., 2017).

During the CLOUD14 experiments, the collision energy was controlled between 62 and 72 Td to reduce the humidity dependence of the methods, as it may complicate the detection of organic compounds. A gas standard mixture containing 1 ppm of 3-hexanone, heptanone, and α pinene in nitrogen was dynamically diluted by a factor of 1000 in VOC-free air to contain 1 ppbv of each compound, and it was then used to calibrate the PTR3-TOF. All data were analyzed using TOF-Tracer software coded using Julia 0.6 (https://github.com/lukasfischer83/TOF-Tracer, last access: 27 August 2024) and were further corrected for the duty-cycle transmission of TOF and temperaturedependent sampling-line losses (Stolzenburg et al., 2018). On the one hand, duty-cycle-corrected counts per second (dcps), dcps_i = cps_i × $(101/m_i)^{1/2}$, were utilized to account for the mass-dependent transmission of the TOF mass spectrometer (Breitenlechner et al., 2017). The calculated sensitivities of 3-hexanone and heptanone were comparable to those observed. Therefore, the concentration of oxygenated products was estimated using the sensitivity of 3-hexanone as lower-limit values due to possible fragmentation (Breitenlechner et al., 2017; Stolzenburg et al., 2018). On the other hand, the detected OOMs with (extremely) low volatility were assumed to be lost by diffusion and were, thus, adjusted by a temperature-dependent loss correction. The samplingline losses considered three loss sections under different temperatures, including losses at the sampling lines within and outside of the chamber and within the PTR3-TOF instrument. Details can be found in previous studies (Breitenlechner et al., 2017; Stolzenburg et al., 2018).

2.5 Product analysis by I⁻-CIMS

The $I^-\text{-}\text{CIMS}$ was capable of characterizing both the gas and particle phases (Lopez-Hilfiker et al., 2014). In the gas-phase mode, gases were directly sampled into a 100 mbar turbulent ion–molecule reactor, while particles were collected onto a polytetrafluoroethylene (PTFE) filter through a separate, dedicated sampling port. Analytes were then ionized with I^- chemical ionization and extracted into a TOF mass analyzer (Wang et al., 2020). The LoD of $I^-\text{-}\text{CIMS}$ for OOMs could be lowered to $\sim 10^7$ molec. cm $^{-3}$ (Lee et al., 2014). In this study, only gas-phase data are reported.

Iodide ions (I $^-$) were used as the reagent ions and formed by passing a 1.0 slpm flow of ultrahigh-purity N $_2$ over a diffusion tube filled with methyl iodide (CH $_3$ I) and then through a 210 Po radioactive source. In the sampling mode, the reagent ion flow was mixed with a sample flow in the IMR at \sim 150 mbar. Coaxial core sampling was used to minimize the vapor wall loss in the sampling line. The total flow was kept at 18.0 slpm and the core flow at 4.5 slpm; the instrument sampled at the center of the core flow with a flow rate of 1.6 slpm. The gas-phase background signal was de-

termined by routinely introducing zero air directly into the inlet. Data were analyzed using Tofware (2.5.11_FIGAERO version; Aerodyne Inc., USA), resulting in 10 s average mass spectra. The ion signal was normalized by the sum of reagent ion signals (i.e., m/Q 127 for I⁻ and 145 for H₂OI⁻).

2.6 Volatility of OOMs

It is challenging to directly measure the vapor pressure of individual OOMs due to the difficulty involved in acquiring authentic standards. To overcome experimental challenges, model calculations have been developed to estimate the vapor pressure using, for example, structure-based and formula-based estimations (Pankow and Asher, 2008). Volatility basis set (VBS) parameterization, a categorization framework based on a quantifiable organic property (i.e., volatility), has been established and is frequently used to characterize oxidation chemistry (Donahue et al., 2011; Li et al., 2016). The VBS parameterization is useful for classifying the wide range of OOMs into multiple volatility groups, including extremely low volatility organic compounds (ELVOCs) and low-volatility organic compounds (LVOCs), based on their effective saturation concentration (C^*) in micrograms per cubic meter (Bianchi et al., 2019). In this study, we applied the VBS parameterization optimized by Isaacman-VanWertz and Aumont (2021; Li et al., 2016):

$$\log_{10}C^{*}(298 \text{ K}) = \left(n_{\text{C}}^{0} - n_{\text{C}}\right)b_{\text{C}} - n_{\text{O}}b_{\text{O}}$$
$$-2\frac{n_{\text{C}}n_{\text{O}}}{(n_{\text{C}} + n_{\text{O}})}b_{\text{CO}} - n_{\text{N}}b_{\text{N}} - n_{\text{S}}b_{\text{S}}, \quad (3)$$

where $n_{\rm C}$, $n_{\rm O}$, $n_{\rm N}$, and $n_{\rm S}$ are the number of carbon, oxygen, nitrogen, and sulfur atoms of the specific molecule, respectively; $n_{\rm C}^0$ is the reference carbon number; $b_{\rm C}$, $b_{\rm O}$, $b_{\rm N}$, and $b_{\rm S}$ are the contribution of each respective atom species to $\log_{10}C^*$; and $b_{\rm CO}$ is the carbon–oxygen nonideality (Donahue et al., 2011). Values of the b coefficient can be found in Li et al. (2016). The formula used to estimate the vapor pressure was amended to convert all NO₃ groups into OH groups to reduce the bias from the compounds containing nitrates (Daumit et al., 2013; Isaacman-VanWertz and Aumont, 2021).

Due to the different temperatures in the CLOUD14 experiments, we adjusted $C^*(298 \,\mathrm{K})$ to the measured experimental temperature as follows:

$$\log_{10}C^{*}(T) = \log_{10}C^{*}(298 \,\mathrm{K}) + \frac{\Delta H_{\text{vap}}}{R \ln(10)} \times \left(\frac{1}{298} - \frac{1}{T}\right),\tag{4}$$

$$\Delta H_{\text{vap}}(\text{kJ mol}^{-1}) = -11 \cdot \log_{10} C^*(298 \,\text{K}) + 129, \tag{5}$$

where T is the temperature in kelvin, $C^*(298 \text{ K})$ is the saturation vapor concentration at 298 K, ΔH_{vap} is the evaporation enthalpy, and R is the gas constant (8.3134 J K⁻¹ mol⁻¹).

The potential presence of isomers may result in uncertainty in this method, as the only input is the compound's molecular formula.

In this study, all oxidation products were grouped into six volatility regimes: ultralow-volatility compounds (ULVOCs, $C^* < 10^{-8.5} \, \mu \mathrm{g \, m^{-3}}$), extremely low volatility compounds (ELVOCs, $10^{-8.5} < C^* < 10^{-4.5} \, \mu \mathrm{g \, m^{-3}}$), low-volatility compounds (LVOCs, $10^{-4.5} < C^* < 10^{-0.5} \, \mu \mathrm{g \, m^{-3}}$), semi-volatile compounds (SVOCs, $10^{-0.5} < C^* < 10^{2.5} \, \mu \mathrm{g \, m^{-3}}$), intermediate-volatility organic compounds (IVOCs, $10^{2.5} < C^* < 10^{6.5} \, \mu \mathrm{g \, m^{-3}}$), and volatile organic compounds (VOCs, $10^{6.5} < C^* \, \mu \mathrm{g \, m^{-3}}$) based on the VBS parameterization.

3 Results and discussions

3.1 Peak identification for the NH₄⁺-Orbitrap

As a promising reagent ion for detecting the full range of OOMs, more ions with low concentration were captured by NH_4^+ , whose identification and quantification were most affected by overlapping signals. The relative intensities of neighboring peaks should also be considered when estimating their ease of separation. It has been shown that a higher mass resolution reduced the interference of adjacent peaks based on NO_3^- or $\mathrm{C}_2\mathrm{H}_3\mathrm{O}_2^-$ reagent ions (Riva et al., 2019a, 2020). Therefore, the ability of the NH_4^+ -Orbitrap to separate overlapping mass spectral peaks was compared to NH_4^+ -TOF.

The mass resolution was defined as the ratio of m to Δm , where m was the mass-to-charge ratio of the analyte ion and Δm was the full width at half maximum (FWHM). Higher mass resolution allows unambiguous mass spectral peak assignment. For a pair of overlapping peaks of equal intensity, the distance between their respective peak center, referred to hereafter simply as peak distance (dm), needed to be greater than approximately 0.8 of the FWHM of the overlapping peaks, such that they could be reasonably deconvolved (as shown in Fig. S2 in the Supplement). Depending on their experience, individuals may be able to visually identify the presence of overlapping peaks at lower or higher dm values. We arbitrarily defined the minimum dm (normalized to that of the FWHM, or Δm) as the value at which the observed spectrum ("Combined" trace in Figs. S2 and S3 in the Supplement) had a local minimum between the centers of the overlapping peaks (i.e., there was a "dip" in the observed signal between ion peaks). The minimum dm value increased with the intensity ratio of overlapping peaks, ranging roughly from 0.85 (for equally intense peaks) to 1.43 (for peaks differing by 1 order of magnitude with respect to their respective intensities), as shown in Fig. S3. In practice, noise and the presence of additional neighboring peaks would further complicate peak deconvolution. For simplicity, we used

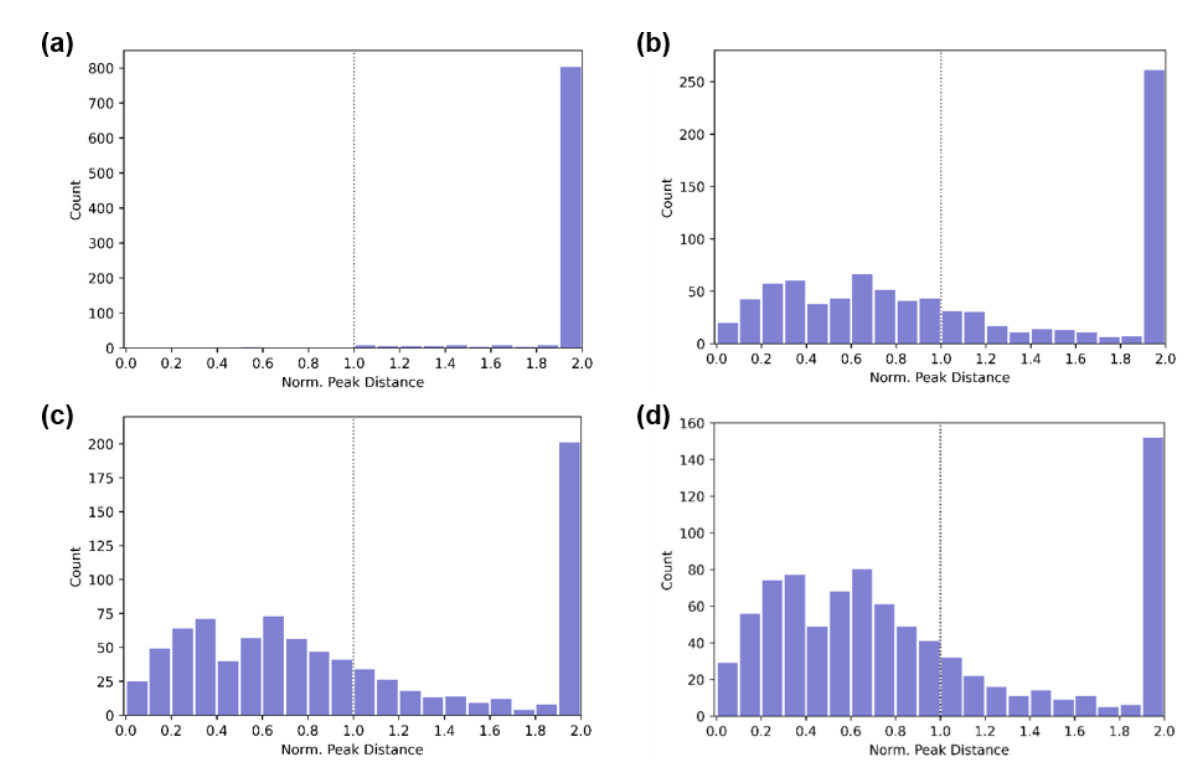


Figure 1. Number of adjacent peaks within an intensity threshold as a function of the normalized peak distance observed by the (a) NH_4^+ - Orbitrap and (b-d) NH_4^+ -TOF. The normalized peak distance was the ratio of the distance between neighboring peaks to the full width at half maximum (FWHM). For each ion, the distance to the closest neighbor with a relative peak intensity that exceeded (a) 20 %, (b) 100 %, (c) 50 %, and (d) 20 % is recorded.

a normalized dm of 1 (i.e., $dm = \Delta m$) as a threshold for the unambiguous deconvolution of the neighboring peaks.

Figure 1 shows the histogram of the distances between neighboring peaks normalized against the FWHM for the NH₄⁺-Orbitrap and the NH₄⁺-TOF with a mass resolution of 10000. In each histogram, one count indicated that an ion had at least one neighboring ion with a relative intensity of 20 %, 50 %, or 100 % (with a higher relative intensity threshold value being less selective). Neighboring ions separated by distances exceeding 2 times the FWHM were considered well separated. For ions with multiple neighboring peaks within the 2 times the FWHM separation distance window, the distance to the first neighboring peak that satisfied the aforementioned relative intensity threshold was reported. Overall, the NH₄⁺-Orbitrap can separate most of the observed ions (> 99 %), while the NH_4^+ -TOF, depending on the relative intensity threshold set, can separate only 32 % to 46 % of all the ions by at least 1 FWHM. It should be noted that the NH₄⁺-Orbitrap has shown its strength with respect to separating neighboring peaks in controlled experiments, in which the knowledge of the chemical compositions for OOMs is relatively abundant. The advantages of a higher mass resolution should be further stressed in ambient observations, where knowledge of OOM species can be limited with a larger number of detectable peaks.

3.2 Characterization of OOMs by four instruments

Figure 2 shows mass defect plots of OOMs measured by the NH₄⁺-Orbitrap, NO₃⁻-LTOF, PTR3-TOF, and I⁻-CIMS, identifying 484, 252, 145, and 67 species, respectively, in run 2211. The NH₄⁺-Orbitrap detected the widest range of products, including HOMs and the less-oxidized species (i.e., O < 6). Out of the 484 compounds, 5 % were amines. The number of O atoms in OOMs varied from 1 to 11 in monomers (C_{2-10}) and from 2 to 16 for dimeric products (C₁₄₋₂₀), with an average elemental oxygen-to-carbon ratio (O:C) of 0.4 ± 0.2 (the value following " \pm " hereafter refers to the standard deviation of O: C during the experiment). As expected, the NO₃-LTOF exhibited a very good sensitivity to HOMs, with the highest O: C of 0.7 ± 0.3 . The PTR3-TOF mainly detected compounds below m/Q 300 Th with an average O : C of 0.5 ± 0.3 , which was due to the optimization (i.e., lowering the ratio of the electric field strength to the sample gas number density value, E/N) to measure ammonia and amines sensitively, which ultimately impacted its capability to efficiently detect OOMs. However, many lessoxygenated OOMs were still observed by the PTR3-TOF and were used to conduct the correlation analysis of time series with those detected by the NH_{Δ}^{+} -Orbitrap. Due to the selectivity and potential losses within the sampling line/in-

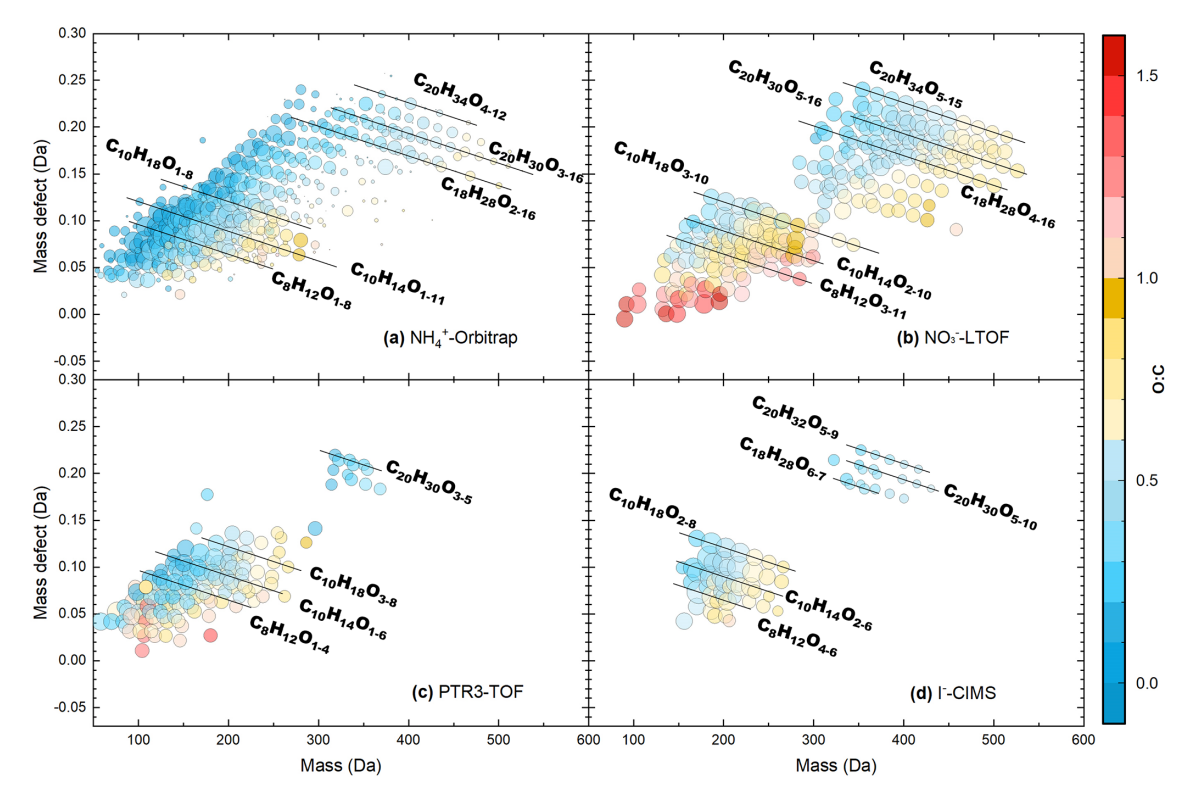


Figure 2. Mass defect plots for organic compounds measured by the (a) NH_4^+ -Orbitrap, (b) NO_3^- -LTOF, (c) PTR3-TOF, and (d) I $^-$ -CIMS in run 2211. The x axis represents the mass-to-charge ratio of the neutral analyte, while the y axis represents the corresponding mass defect, which is the difference between their exact mass and nominal mass (Schobesberger et al., 2013). Markers are all sized by the logarithm of their corresponding signals and colored by the O: C value. Some major OOMs measured by different instruments are indicated by the black lines.

let of the I⁻-CIMS equipped with a FIGAERO inlet, fewer monomers of C_{8-10} and dimers of C_{19-20} were observed, with an average O: C of 0.5 ± 0.2 .

3.3 Instrumental comparisons: correlations

Due to differences in the selectivity and sensitivity of the analytical methods toward OOMs, ~42 % of species identified by the NH₄⁺-Orbitrap were simultaneously detected by other mass spectrometers (Fig. S4 in the Supplement). To identify how the NH₄⁺-Orbitrap performed compared to the other mass spectrometers, a correlation analysis including all co-detected ions was complied. The experimental conditions of the runs used for performing this analysis are summarized in Table S1 in the Supplement. The dataset covered a variety of conditions, such as different concentrations of α -pinene, NO_x, SO₂, and CO as well as the level of RH. The R^2 value was calculated using the time series of OOMs with the same elemental composition measured by the different mass spectrometers. Figure 3 displays the correlation coefficient of time series for the detected compounds, with the marker size scaled by the R^2 value. The NH_4^+ -Orbitrap and the NO₃-LTOF-detected OOMs with the same chemical compositions, covering monomers and dimers, among which 18 OOMs showed $R^2 > 0.9$. Regarding the PTR3-TOF, the NH₄⁺-Orbitrap demonstrated high correlations for most of the monomers and a few dimers, including 32 species with an $R^2 > 0.9$. Due to potential losses within the FIGAERO inlet, fewer OOMs were detected by the I⁻-CIMS. However, certain families of compounds, including C₁₀H₁₅O₅₋₇N and C₂₀H₃₁O_{7,9}N, showed high correlations (i.e., $R^2 > 0.9$) between the NH₄⁺-Orbitrap and the I⁻-CIMS. Finally, the NO₃⁻-LTOF was regarded as the reference instrument for HOM measurements. Only a few monomers with a high oxygen content were detected by the NO₃⁻-LTOF and the PTR3-TOF, and only a few dimers were detected between the NO₃⁻-LTOF and the I⁻-CIMS, with moderate relevance.

The fact that the correlations of certain molecules are lower than 0.9 may be due to the molecules' composition or potential ionization artifacts. RH dependence is an important property leading to the low correlations, as the experiment includes RH variation from 20 % to 80 %. Although NO_3^- ion chemistry had been reported to be less dependent on RH (Viggiano et al., 1997), the sensitivities of the PTR3-TOF (Breitenlechner et al., 2017) and I^- -CIMS (Lee et al., 2014) both showed high dependence on RH. In addition, the relative sensitivity of the NH_4^+ -Orbitrap was also influenced by varying RH (see details in Sect. 3.6). Fragmentation, such as

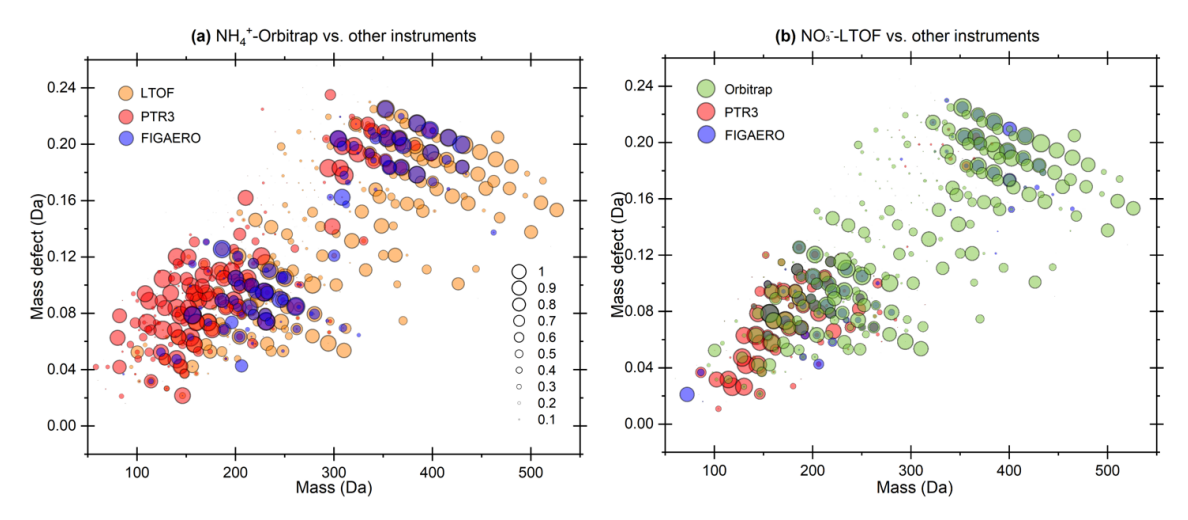


Figure 3. Mass defect plots depicting the compounds for which a time-series correlation was observed by the (a) NH_4^+ -Orbitrap and (b) NO_3^- -LTOF with other MS instruments. Each circle represents a molecule, while marker size represents the correlation (R^2) of the time series of the molecules between two different MS instruments. Two sets of data in run 2211 and 2213 were used to reduce uncertainties.

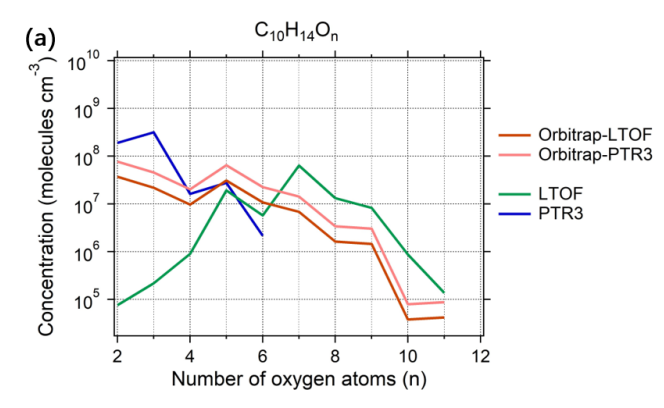
the decomposition of dimers, would also lead to low correlations. However, less fragmentation is expected to occur in the NH₄⁺-Orbitrap using similar settings to those employed in our earlier studies (Riva et al., 2019a, 2020). In comparison, the decomposition of peroxides (i.e., ROOR and ROOH) can be expected within the PTR3-TOF. While the fragmentation of dimeric compounds can contribute to the overall signal of the monomers, the concentration of such species remains minor (Li et al., 2022). As a result, no large enhancement of the monomers' signal intensity is expected. There are also other artifacts that cannot be excluded based on the current dataset, including potential isomers and differences in the response time between instruments, which would also lead to the low correlations. However, by comparing the coverage regions of the instruments under multiple experimental conditions, the NH₄⁺-Orbitrap was capable of covering the widest range of compounds and showed overall good agreement with other mass spectrometers.

3.4 Instrumental comparisons: concentration estimates

Concentrations of the identified compounds were estimated for the NH₄⁺-Orbitrap, as described in Sect. 2.2. The sensitivity of the NH₄⁺-Orbitrap was constrained based on the intensity comparison between it and the other two instruments. For instance, concentrations of the most abundant C_{10} monomers (i.e., $C_{10}H_{14/16}O_n$) were estimated using different calibration factors (Fig. 4), which were measured under steady-state conditions (i.e., run 2211 with $[O_3] = 100\,\mathrm{ppbv}$ and $[\alpha\mathrm{-pinene}] = 2\,\mathrm{ppbv}$ at $\mathrm{RH} = 10\,\%$). The concentrations of C_{10} monomers measured by the NH₄⁺-Orbitrap based on the two calibration factors vary within a factor of 2, which indicates consistency between the two correlation analyses. The variation trend in the concentrations with the oxygen number of the NH₄⁺-Orbitrap is sim-

ilar to that of the NO_3^- -LTOF in the range of $n_0 > 6$ and similar to that of the PTR3-TOF in the range of $n_0 = 1-5$. Considering that such ranges are also the oxygen number ranges with high sensitivities, this proves the robustness of the NH₄⁺-Orbitrap and the intensity-based relative comparison between the NH₄⁺-Orbitrap and two reference instruments. As previously reported, the Orbitrap mass analyzer had a nonlinear response to compounds present at extremely low concentrations, which was independent of the sample composition, instrumental setup, or reagent ion (Riva et al., 2020; Cai et al., 2022). A similar evaluation was performed for the NH₄⁺-Orbitrap by comparing the measured vs. the theoretical isotopic intensities. As shown in Fig. S5 in the Supplement, the NH₄⁺-Orbitrap had a linear response for an ion intensity greater than $\sim 5 \times 10^3$ cps, which corresponded to a limit of quantification (LoQ; consistent with the lowest normalized signal observed within the linear range) of $\sim 5 \times 10^5$ molec. cm⁻³ for OOMs, estimated using the calibration factor derived from the NO₃-LTOF; this is consistent with a previous study (Riva et al., 2020).

Figure 5 presents the concentrations of all OOMs measured by the NH_4^+ -Orbitrap and determined by applying two different calibration factors. The concentrations of OOMs measured by the NH_4^+ -Orbitrap were higher than both the NO_3^- -LTOF and the PTR3-TOF, the latter of which was optimized for measuring ammonia and amines. This indicates that the NH_4^+ -Orbitrap can provide a better constraint on the concentrations of the primary products. As an example, pinonaldehyde (i.e., $C_{10}H_{16}O_2$), as one of the most abundant oxidation products, was not efficiently detected by the NO_3^- -LTOF, which is consistent with the higher selectivity of the NO_3^- reagent ion. To further illustrate the selectivity of the different reagent ions, Fig. 6 offers a summary of the performance of each mass spectrometer with respect to their abil-



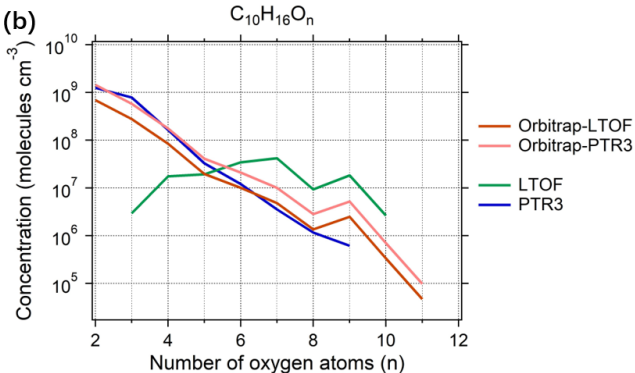


Figure 4. Estimated concentrations of the main C_{10} oxidation products (a) $C_{10}H_{14}O_n$ and (b) $C_{10}H_{16}O_n$ as a function of the oxygen numbers observed in run 2211. The Orbitrap-LTOF and Orbitrap-PTR3 represented the estimated concentration of monomers measured by the NH_4^+ -Orbitrap using the calibration factors from the correlation analysis with the NO_3^- -LTOF and PTR3-TOF, respectively.

ity to detect monomeric compounds, such as $C_{10}H_{16}O_n$. The y axis is arbitrary and represents a qualitative characterization of the oxygen content when compounds were detected by different CI schemes. Similar to previous results, the I⁻-CIMS detected OOMs with $n_{\rm O} > 3$ but was not optimal for the detection of monomers with $n_{\rm O} > 7$ (Riva et al., 2019b). The NO₃-LTOF was mainly selective towards HOMs with $n_{\rm O} > 6$ (Riva et al., 2019b). The PTR3-TOF had limited capabilities with respect to detecting OOMs with $n_{\rm O} > 5$ due to the optimization of the instrument to obtain a very sensitive measurement of ammonia. Previously, the amine-CI demonstrated promise for the detection of OOMs, but this was limited to applications under comparatively clean conditions due to a considerable depletion of the reagent ion and the presence of overlapping peaks (Berndt et al., 2018b; Riva et al., 2019b). While showing a similar OOM detection range to the amine-CI, the NH₄⁺-CI, in tandem with the greater mass resolution of the Orbitrap mass analyzer, provided a linear response to higher loading. As shown in Fig. S6 in the Supplement, background peaks were not affected by atmospherically relevant concentrations of O_3 and α -pinene. Overall,

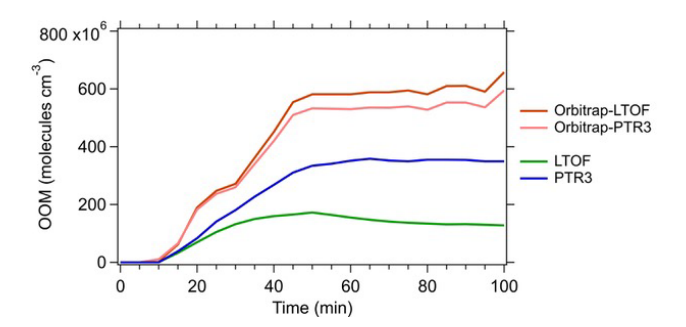


Figure 5. Estimated concentrations of all measured OOMs in the photooxidation of α-pinene. All C_{8-10} monomers and C_{18-20} dimers measured by the NH₄⁺-Orbitrap, NO₃⁻-LTOF, and PTR3-TOF in run 2213 were summed up. The concentrations of OOMs measured by the NH₄⁺-Orbitrap were quantified by the calibration factors derived from a correlation analysis between the NH₄⁺-Orbitrap and the NO₃⁻-LTOF (Orbitrap-LTOF, light green) or the PTR3-TOF (Orbitrap-PTR3, light blue), respectively.

the NH₄⁺-Orbitrap appears to have the potential to provide a more reliable identification and quantification of OOMs produced from VOC oxidation compared with other existing mass spectrometry techniques.

3.5 Volatility distribution by four instruments

Figure 7 shows the distribution of oxidation products measured by four MS instruments according to their saturation vapor concentrations ($log_{10}C_{sat}$) estimated using a volatility parameterization (Li et al., 2016; Isaacman-VanWertz and Aumont, 2021). OOMs were grouped into the following six volatility regimes based on a volatility basis set (VBS) parameterization: ultralow-volatility organic compounds (ULVOCs), extremely low volatility organic compounds (ELVOCs), low-volatility organic compounds (LVOCs), semi-volatile organic compounds (SVOCs), intermediatevolatility organic compounds (IVOC), and volatile organic compounds (VOCs). ULVOCs and ELVOCs initiate cluster growth and form new particles. The total signal in each volatility bin represented the sum of the signal intensity of OOMs within the volatility range. The mean contributions of these compound regimes are shown in the VBS pie charts. The ULVOC, ELVOC, and LVOC regimes were well captured by NH₄⁺-Orbitrap and NO₃⁻-LTOF. The PTR3-TOF only characterized the SVOC and IVOC regimes (along with VOCs). The IVOC and VOC regimes in the PTR3-TOF and NH₄⁺-Orbitrap were generally less-oxygenated VOCs (i.e., $n_{\rm O}$ < 5). IVOCs comprised the biggest mass contributions for the NH₄⁺-Orbitrap, whereas LVOCs dominated in the NO_3^- -LTOF. Hence, the detection of the NH_4^+ -Orbitrap covered the widest range of volatilities, clearly highlighting the benefit of using this technique for the formation and fate of OOMs. In the past, reagent switching has not been practical, and users would run multiple mass spectrometer systems

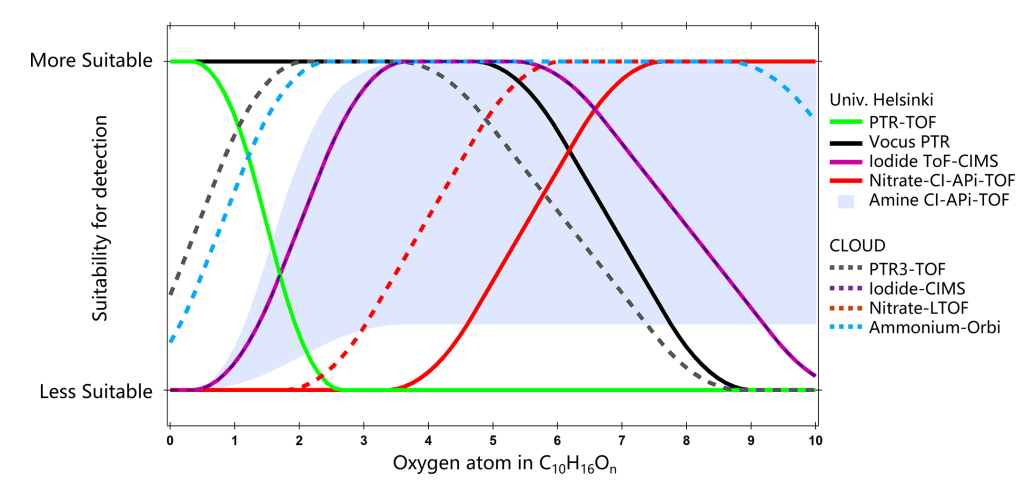


Figure 6. Estimated detection suitability of the different CIMS techniques for monomers from α -pinene ozonolysis, plotted as a function of the number of oxygen atoms. Image modified from Riva et al. (2019b).

in parallel or use a Multi-scheme chemical IONization inlet (MION) with only one mass spectrometer to obtain the fullest possible mass spectrum (Rissanen et al., 2019; Huang et al., 2021). Using the NH_4^+ -Orbitrap, it is now possible to cover the entire range of compounds, which is not the case with most CI techniques.

3.6 RH dependance of the NH₄⁺-Orbitrap

The sensitivity of the reagent-adduct ionization has been reported to be affected by the presence of water vapor for a variety of reagent ions (Lee et al., 2014; Breitenlechner et al., 2017). The impact of the RH on the detection of OOMs by the NH₄⁺-Orbitrap was also studied. While the concentrations of the gas-phase precursor and oxidant remained constant, the RH was raised from 10 % to 80 %. During this increase, the signal of organic vapor behaved inconsistently under an otherwise constant gas-phase production rate (Surdu et al., 2023) and an increase in the condensation sink (Fig. S7 in the Supplement). As shown in Fig. 8, the NH₄⁺-Orbitrap demonstrated RH dependence. For instance, the signal of less-oxygenated molecules (i.e., $n_{\rm O}$ < 5) increased with increasing RH, especially compounds with $n_{\rm C} = 8$, while the signal of highly oxygenated molecules (i.e., $n_{\rm O} > 10$) decreased as a function of RH. The average behavior of all C₈₋₁₀ monomers and C₁₈₋₂₀ dimers was summarized and compared between four instruments (Fig. S8 in the Supplement). The other three mass spectrometers also showed obvious RH dependence. Similar to the NH₄⁺-Orbitrap, OOMs with $n_{\rm O}$ < 5 measured by the NO₃⁻-LTOF and PTR3-TOF increased at high RH, HOMs with $n_0 > 11$ decreased with RH, and OOMs with $n_{\rm O} = 8 \sim 11$ seemed to be independent of RH. The large variations in OOM intensity measured by the NH₄⁺-Orbitrap at different RH levels may be due to the widest range of oxygen atoms. For OOMs with different oxygen numbers, their varying trends with RH show different characteristics; however, the reasons for this are still not clear. Here, multiple possible reasons are provided to explain the signal evolution of the ions with changing RH, such as water affecting the ionization efficiency or altering the physicochemical processes of the gas-phase chemistry.

First, the efficiency of a particular compound partly relied on whether water vapor competes with the ammonium ion, lowering the sensitivity, or whether it acted as a third body to stabilize the ammonium-organic analyte cluster by removing extra energy from the collision, raising the sensitivity (Lee et al., 2014). Ammonium primary ions can cluster with water molecules when humidity increases, thereby reducing the clustering of NH₄⁺ with organic analytes (Breitenlechner et al., 2017). However, the formed $NH_4^+X_n$ (where X is NH₃ or H₂O; n = 1,2) clusters might also act as reagent ions and ionize OOMs through ligand switching reactions, which were expected to be fast and, thus, improve the charging efficiency (Hansel et al., 2018). Compared with previous NH₄⁺-CIMS results, the $NH_4^+X_n$ reagent ions were expected to be larger due to the absence of the field in the ion-molecule reaction zone in the Orbitrap, resulting in greater ligand exchange and increasing the sensitivity to less-oxygenated species (Canaval et al., 2019).

Despite the influence of water vapor on ionization efficiency in the NH_4^+ -Orbitrap, RH variation could also influence the physicochemical processes (e.g., multiphase chemistry and partitioning). The increase in the condensation sink with increasing RH might lead to a higher loss of OOMs, especially for OOMs with higher oxygen numbers, and thus lower volatility, which might be the main cause of the varying RH dependency with the oxygen number (as shown in Fig. S8). Another potential influential factor is the presence of water in certain chemical reactions, such as reactions with the Criegee intermediates, H_2O/OH chemistry, or multiphase chemistry. For example, although the $C_{10}H_{16}O_{4,5}$ signal detected by NO_3^- -LTOF decreases with increasing RH (Surdu

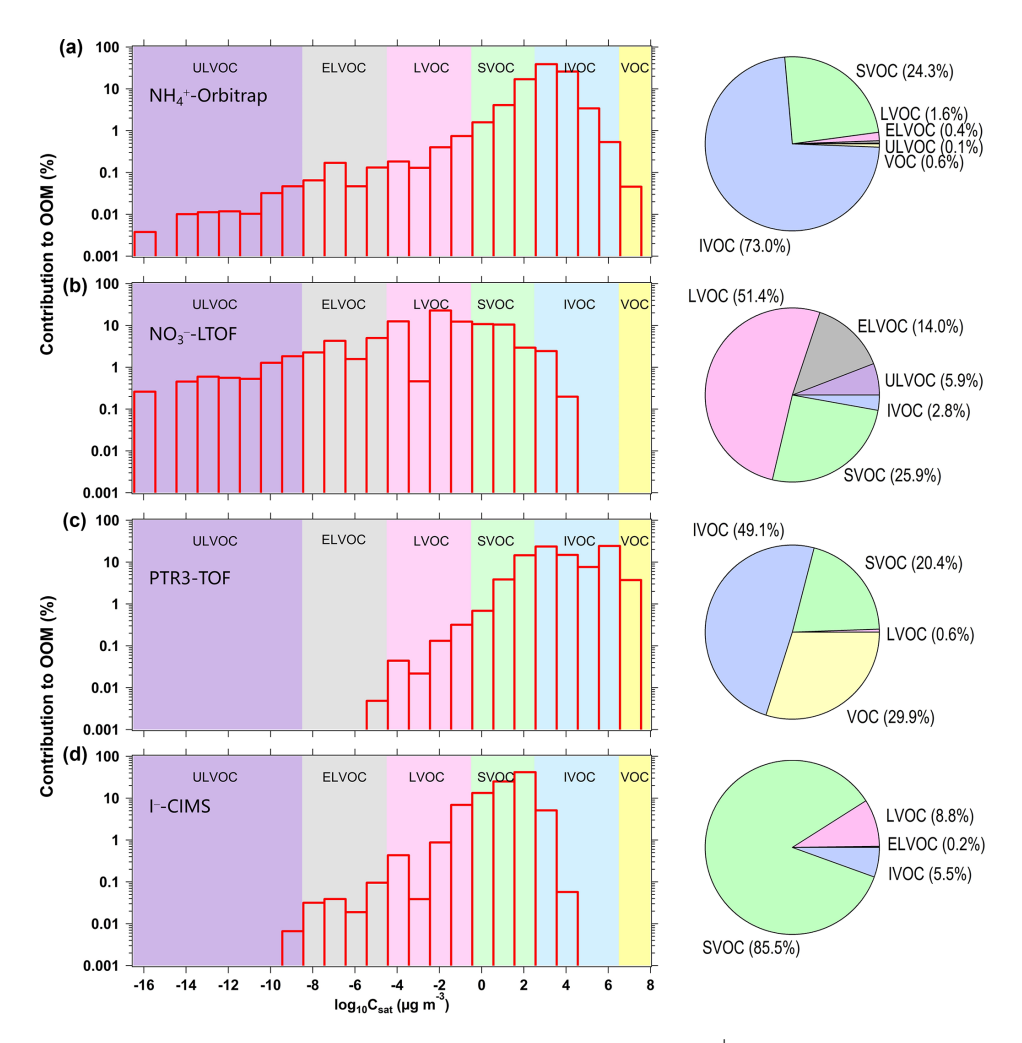


Figure 7. Volatility distribution comparison for organic compounds detected by the (a) NH_4^+ -Orbitrap, (b) NO_3^- -LTOF, (c) PTR3-TOF, and (d) I^- -CIMS. The background colors represent the saturation concentration (C_{sat}) in the range of ultralow-volatility compounds (ULVOCs, purple), extremely low volatility compounds (ELVOCs, gray), low-volatility compounds (LVOCs, pink), semi-volatile compounds (SVOCs, green), intermediate-volatility compounds (IVOCs, blue), and volatile organic compounds (VOCs). The pie charts are the corresponding contributions of the respective VOC, IVOC, SVOC, LVOC, ELVOC, and ULVOC classes in run 2211. Concentrations were used to calculate the contribution in each volatility bin for the NO_3^- -LTOF and PTR3-TOF, while signals were calculated for the NH_4^+ -Orbitrap and I^- -CIMS.

et al., 2023), the summed signal of $C_{8-10}H_{12-18}O_{4-5}$ increased (Fig. S8), which might indicate C–C bond cleavage during the RH increase process (Pospisilova et al., 2020). However, thus far, no clear evidence has been identified; therefore, the accurate reasons for this need to be further verified in target control experiments, such as changing the RH in the IMR of the CI inlet.

4 Summary

In conclusion, this study presented an intercomparison between the NH_4^+ -Orbitrap, NO_3^- -LTOF, PTR3-TOF, and I⁻-CIMS based on the identification and quantification of OOMs formed from the ozonolysis of α -pinene under various environmental conditions. We used NH_4^+ adduct ions

with the Orbitrap mass spectrometer to measure oxygenated species for the first time. The NH₄⁺-Orbitrap is a promising CIMS technique for the comprehensive measurement of the whole product distribution and provides a more complete understanding of the molecular composition and volatility of OOMs. This allows the NH₄⁺-Orbitrap to better monitor the evolution of organic compounds, which can be beneficial for air quality, pollutant transport, and climate models. It is worth noting that NH₄⁺-Orbitrap is not only useful for laboratory-based studies but also for field observations, with the ability to provide a deeper understanding of atmospheric oxidation processes. However, it remains challenging to accurately quantify the concentrations of OOMs due to the absent signals of reagent ions. In addition, RH influences the NH₄⁺-Orbitrap sensitivity, and this impact can be different for

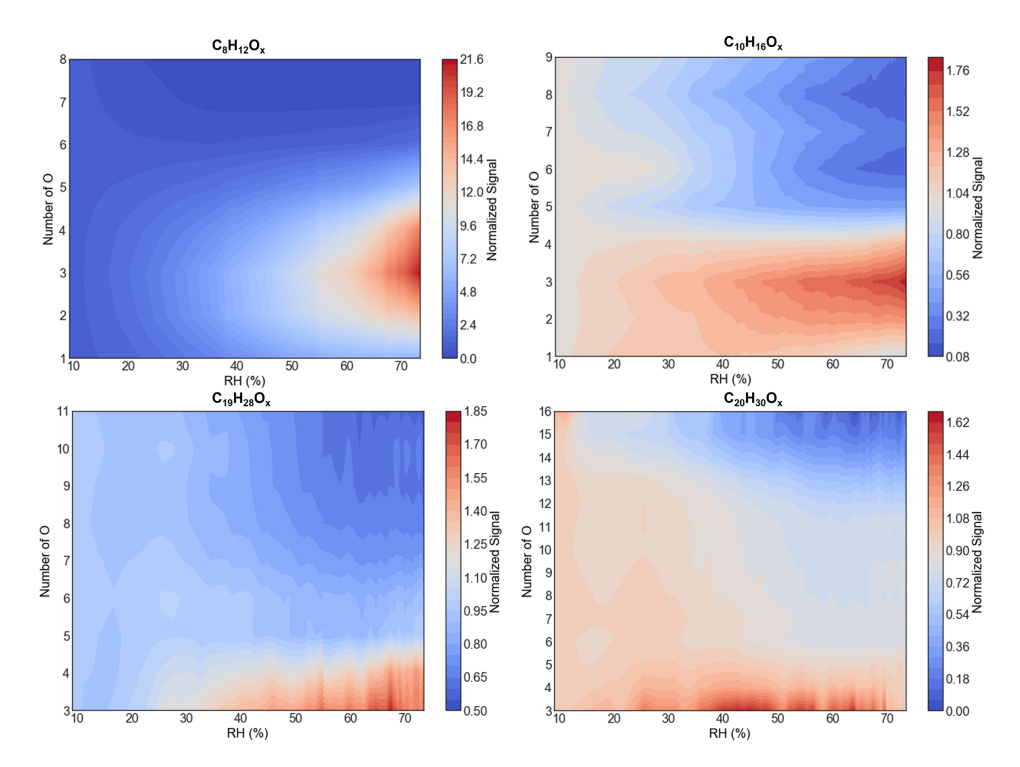


Figure 8. The effect of relative humidity on the distribution of the most abundant monomers and dimers measured by the NH₄⁺-Orbitrap. The RH was ramped from $\sim 10\%$ to $\sim 80\%$ in run 2211. The normalized signal represents the signal variation ratio at certain RH levels compared to that at RH = 10%, normalized signal = $\frac{\text{signal}_{RH}}{\text{signal}_{10\%}}$.

each OOM. Therefore, this specific effect requires more attention via dedicated studies (e.g., the injection of pure standards or a mixture of standards in an atmospheric chamber under various RH conditions) before the NH₄⁺-Orbitrap can be used in field studies. Based on the findings presented here, understanding of the effect of RH on the NH₄⁺-Orbitrap's capabilities is too scarce to be able to comprehend the timeseries evolution of OOMs that would be obtained in the real atmosphere.

Data availability. Data are available upon request from the corresponding author.

Supplement. The supplement related to this article is available online at: https://doi.org/10.5194/amt-17-5413-2024-supplement.

Author contributions. DL, DW, LC, WS, MW, ST, GM, MS, EE, XG, LGC, MG, JP, BR, BS, PR, SP, AH, JC, JK, NMD, CG, IEH, and MR prepared the CLOUD facility or measuring instruments. DL, DW, LC, WS, MW, ST, GM, MS, EE, XG, LGC, MG, JP, BR, BS, JK, and MR collected the CLOUD data. DL, DW, LC, WS, MW, GM, and MR analyzed the data. DL, DW, MW, NMD, CG, IEH, and MR wrote the manuscript and contributed to the scientific

discussion. All authors discussed the results and commented on the paper.

Competing interests. At least one of the (co-)authors is a member of the editorial board of Atmospheric Measurement Techniques. The peer-review process was guided by an independent editor, and the authors also have no other competing interests to declare.

Disclaimer. Publisher's note: Copernicus Publications remains neutral with regard to jurisdictional claims made in the text, published maps, institutional affiliations, or any other geographical representation in this paper. While Copernicus Publications makes every effort to include appropriate place names, the final responsibility lies with the authors.

Acknowledgements. We thank the European Organization for Nuclear Research (CERN) for supporting CLOUD via the provision of important technical and financial resources. We thank the Orbitool team for developing the tools to analyze the mass spectra. This work was financially supported by the French National program LEFE (Les Enveloppes Fluides et l'Environnement), the European Research Council (ERC-StG MAARvEL; grant no. 852161), the European Union's Horizon 2020 Research and Innovation program (Marie Skłodowska-Curie grant nos. 764991 and 701647), the Swiss National Sci-

ence Foundation (grant nos. 200021_169090, 200020_172602, 20FI20_172622, and 206021_198140), the US National Science Foundation (grant nos. NSF_AGS_1801280, NSF_AGC_1801574, NSF_AGS_1801897, and NSF_AGS_2132089), and the German Federal Ministry of Education and Research (grant no. CLOUD-16 01LK1601A). Dandan Li is grateful to the China Scholarship Council for a PhD grant. Mingyi Wang acknowledges financial support from the Schmidt Science Fellows program, Schmidt Futures, in partnership with the Rhodes Trust.

Financial support. This research has been supported by the European Union's Horizon 2020 program (grant nos. 852161, 764991, and 701647), the Schweizerischer Nationalfonds zur Förderung der wissenschaftlichen Forschung (grant nos. 200021_169090, 200020_172602, 20FI20_172622, and 206021_198140), the National Science Foundation (grant nos. NSF_AGS_1801280, NSF_AGC_1801574, NSF_AGS_1801897, and NSF_AGS_2132089), and the Bundesministerium für Bildung und Forschung (grant no. CLOUD-16 01LK1601A).

Review statement. This paper was edited by Bin Yuan and reviewed by two anonymous referees.

References

- Berndt, T., Mentler, B., Scholz, W., Fischer, L., Herrmann, H., Kulmala, M., and Hansel, A.: Accretion Product Formation from Ozonolysis and OH Radical Reaction of α-Pinene: Mechanistic Insight and the Influence of Isoprene and Ethylene, Environ. Sci. Technol., 52, 11069–11077, https://doi.org/10.1021/acs.est.8b02210, 2018a.
- Berndt, T., Scholz, W., Mentler, B., Fischer, L., Herrmann, H., Kulmala, M., and Hansel, A.: Accretion Product Formation from Self- and Cross-Reactions of RO₂ Radicals in the Atmosphere, Angew. Chem. Int. Edit., 57, 3820–3824, https://doi.org/10.1002/anie.201710989, 2018b.
- Bianchi, F., Kurtén, T., Riva, M., Mohr, C., Rissanen, M. P., Roldin, P., Berndt, T., Crounse, J. D., Wennberg, P. O., Mentel, T. F., Wildt, J., Junninen, H., Jokinen, T., Kulmala, M., Worsnop, D. R., Thornton, J. A., Donahue, N., Kjaergaard, H. G., and Ehn, M.: Highly Oxygenated Organic Molecules (HOM) from Gas-Phase Autoxidation Involving Peroxy Radicals: A Key Contributor to Atmospheric Aerosol, Chem. Rev., 119, 3472–3509, https://doi.org/10.1021/acs.chemrev.8b00395, 2019.
- Bianchi, F., Tröstl, J., Junninen, H., Frege, C., Henne, S., Hoyle, C. R., Molteni, U., Herrmann, E., Adamov, A., Bukowiecki, N., Chen, X., Duplissy, J., Gysel, M., Hutterli, M., Kangasluoma, J., Kontkanen, J., Kürten, A., Manninen, H. E., Münch, S., Peräkylä, O., Petäjä, T., Rondo, L., Williamson, C., Weingartner, E., Curtius, J., Worsnop, D. R., Kulmala, M., Dommen, J., and Baltensperger, U.: New particle formation in the free troposphere: A question of chemistry and timing, Science, 352, 1109–1112, https://doi.org/10.1126/science.aad5456, 2016.
- Breitenlechner, M., Fischer, L., Hainer, M., Heinritzi, M., Curtius, J., and Hansel, A.: PTR3: An Instrument for Studying the Lifecycle of Reactive Organic Carbon in the Atmosphere, Anal. Chem.,

- 89, 5824–5831, https://doi.org/10.1021/acs.analchem.6b05110, 2017.
- Cai, R., Li, Y., Clément, Y., Li, D., Dubois, C., Fabre, M., Besson, L., Perrier, S., George, C., Ehn, M., Huang, C., Yi, P., Ma, Y., and Riva, M.: Orbitool: a software tool for analyzing online Orbitrap mass spectrometry data, Atmos. Meas. Tech., 14, 2377–2387, https://doi.org/10.5194/amt-14-2377-2021, 2021.
- Cai, R., Huang, W., Meder, M., Bourgain, F., Aizikov, K., Riva, M., Bianchi, F., and Ehn, M.: Improving the Sensitivity of Fourier Transform Mass Spectrometer (Orbitrap) for Online Measurements of Atmospheric Vapors, Anal. Chem., 94, 15746–15753, https://doi.org/10.1021/acs.analchem.2c03403, 2022.
- Canaval, E., Hyttinen, N., Schmidbauer, B., Fischer, L., and Hansel, A.: NH⁺ Association and Proton Transfer Reactions With a Series of Organic Molecules, Front. Chem., 7, 191, https://doi.org/10.3389/fchem.2019.00191, 2019.
- Caudillo, L., Rörup, B., Heinritzi, M., Marie, G., Simon, M., Wagner, A. C., Müller, T., Granzin, M., Amorim, A., Ataei, F., Baalbaki, R., Bertozzi, B., Brasseur, Z., Chiu, R., Chu, B., Dada, L., Duplissy, J., Finkenzeller, H., Gonzalez Carracedo, L., He, X.-C., Hofbauer, V., Kong, W., Lamkaddam, H., Lee, C. P., Lopez, B., Mahfouz, N. G. A., Makhmutov, V., Manninen, H. E., Marten, R., Massabò, D., Mauldin, R. L., Mentler, B., Molteni, U., Onnela, A., Pfeifer, J., Philippov, M., Piedehierro, A. A., Schervish, M., Scholz, W., Schulze, B., Shen, J., Stolzenburg, D., Stozhkov, Y., Surdu, M., Tauber, C., Tham, Y. J., Tian, P., Tomé, A., Vogt, S., Wang, M., Wang, D. S., Weber, S. K., Welti, A., Yonghong, W., Yusheng, W., Zauner-Wieczorek, M., Baltensperger, U., El Haddad, I., Flagan, R. C., Hansel, A., Höhler, K., Kirkby, J., Kulmala, M., Lehtipalo, K., Möhler, O., Saathoff, H., Volkamer, R., Winkler, P. M., Donahue, N. M., Kürten, A., and Curtius, J.: Chemical composition of nanoparticles from α -pinene nucleation and the influence of isoprene and relative humidity at low temperature, Atmos. Chem. Phys., 21, 17099-17114, https://doi.org/10.5194/acp-21-17099-2021, 2021.
- Daumit, K. E., Kessler, S. H., and Kroll, J. H.: Average chemical properties and potential formation pathways of highly oxidized organic aerosol, Faraday Discuss., 165, 181–202, https://doi.org/10.1039/c3fd00045a, 2013.
- Donahue, N. M., Epstein, S. A., Pandis, S. N., and Robinson, A. L.: A two-dimensional volatility basis set: 1. organic-aerosol mixing thermodynamics, Atmos. Chem. Phys., 11, 3303–3318, https://doi.org/10.5194/acp-11-3303-2011, 2011.
- Ehn, M., Junninen, H., Petäjä, T., Kurtén, T., Kerminen, V.-M., Schobesberger, S., Manninen, H. E., Ortega, I. K., Vehkamäki, H., Kulmala, M., and Worsnop, D. R.: Composition and temporal behavior of ambient ions in the boreal forest, Atmos. Chem. Phys., 10, 8513–8530, https://doi.org/10.5194/acp-10-8513-2010, 2010.
- Ehn, M., Thornton, J. A., Kleist, E., Sipila, M., Junninen, H., Pullinen, I., Springer, M., Rubach, F., Tillmann, R., Lee, B., Lopez-Hilfiker, F., Andres, S., Acir, I. H., Rissanen, M., Jokinen, T., Schobesberger, S., Kangasluoma, J., Kontkanen, J., Nieminen, T., Kurten, T., Nielsen, L. B., Jorgensen, S., Kjaergaard, H. G., Canagaratna, M., Maso, M. D., Berndt, T., Petaja, T., Wahner, A., Kerminen, V. M., Kulmala, M., Worsnop, D. R., Wildt, J., and Mentel, T. F.: A large source of low-volatility secondary organic aerosol, Nature, 506, 476–479, https://doi.org/10.1038/nature13032, 2014.

- Fan, J., Wang, Y., Rosenfeld, D., and Liu, X.: Review of Aerosol–Cloud Interactions: Mechanisms, Significance, and Challenges, J. Atmos. Sci., 73, 4221–4252, https://doi.org/10.1175/jas-d-16-0037.1, 2016.
- Hallquist, M., Wenger, J. C., Baltensperger, U., Rudich, Y., Simpson, D., Claeys, M., Dommen, J., Donahue, N. M., George, C., Goldstein, A. H., Hamilton, J. F., Herrmann, H., Hoffmann, T., Iinuma, Y., Jang, M., Jenkin, M. E., Jimenez, J. L., Kiendler-Scharr, A., Maenhaut, W., McFiggans, G., Mentel, Th. F., Monod, A., Prévôt, A. S. H., Seinfeld, J. H., Surratt, J. D., Szmigielski, R., and Wildt, J.: The formation, properties and impact of secondary organic aerosol: current and emerging issues, Atmos. Chem. Phys., 9, 5155–5236, https://doi.org/10.5194/acp-9-5155-2009, 2009.
- Hansel, A., Scholz, W., Mentler, B., Fischer, L., and Berndt, T.: Detection of RO₂ radicals and other products from cyclohexene ozonolysis with NH₄⁺ and acetate chemical ionization mass spectrometry, Atmos. Environ., 186, 248–255, https://doi.org/10.1016/j.atmosenv.2018.04.023, 2018.
- Haywood, J. and Boucher, O.: Estimates of the direct and indirect radiative forcing due to tropospheric aerosols: A review, Rev. Geophys., 38, 513–543, https://doi.org/10.1029/1999rg000078, 2000.
- Heinritzi, M., Simon, M., Steiner, G., Wagner, A. C., Kürten, A., Hansel, A., and Curtius, J.: Characterization of the massdependent transmission efficiency of a CIMS, Atmos. Meas. Tech., 9, 1449–1460, https://doi.org/10.5194/amt-9-1449-2016, 2016.
- Huang, W., Li, H., Sarnela, N., Heikkinen, L., Tham, Y. J., Mikkilä, J., Thomas, S. J., Donahue, N. M., Kulmala, M., and Bianchi, F.: Measurement report: Molecular composition and volatility of gaseous organic compounds in a boreal forest from volatile organic compounds to highly oxygenated organic molecules, Atmos. Chem. Phys., 21, 8961–8977, https://doi.org/10.5194/acp-21-8961-2021, 2021.
- Isaacman-VanWertz, G. and Aumont, B.: Impact of organic molecular structure on the estimation of atmospherically relevant physicochemical parameters, Atmos. Chem. Phys., 21, 6541–6563, https://doi.org/10.5194/acp-21-6541-2021, 2021.
- Jimenez, J. L., Canagaratna, M. R., Donahue, N. M., Prevot, A. S. H., Zhang, Q., Kroll, J. H., DeCarlo, P. F., Allan, J. D., Coe, H., Ng, N. L., Aiken, A. C., Docherty, K. S., Ulbrich, I. M., Grieshop, A. P., Robinson, A. L., Duplissy, J., Smith, J. D., Wilson, K. R., Lanz, V. A., Hueglin, C., Sun, Y. L., Tian, J., Laaksonen, A., Raatikainen, T., Rautiainen, J., Vaattovaara, P., Ehn, M., Kulmala, M., Tomlinson, J. M., Collins, D. R., Cubison, M. J., Dunlea, J., Huffman, J. A., Onasch, T. B., Alfarra, M. R., Williams, P. I., Bower, K., Kondo, Y., Schneider, J., Drewnick, F., Borrmann, S., Weimer, S., Demerjian, K., Salcedo, D., Cottrell, L., Griffin, R., Takami, A., Miyoshi, T., Hatakeyama, S., Shimono, A., Sun, J. Y., Zhang, Y. M., Dzepina, K., Kimmel, J. R., Sueper, D., Jayne, J. T., Herndon, S. C., Trimborn, A. M., Williams, L. R., Wood, E. C., Middlebrook, A. M., Kolb, C. E., Baltensperger, U., and Worsnop, D. R.: Evolution of Organic Aerosols in the Atmosphere, Science, 326, 1525-1529, https://doi.org/10.1126/science.1180353, 2009.
- Jokinen, T., Sipilä, M., Junninen, H., Ehn, M., Lönn, G., Hakala, J., Petäjä, T., Mauldin III, R. L., Kulmala, M., and Worsnop, D. R.: Atmospheric sulphuric acid and neutral cluster measure-

- ments using CI-APi-TOF, Atmos. Chem. Phys., 12, 4117–4125, https://doi.org/10.5194/acp-12-4117-2012, 2012.
- Kirkby, J., Duplissy, J., Sengupta, K., Frege, C., Gordon, H., Williamson, C., Heinritzi, M., Simon, M., Yan, C., Almeida, J., Tröstl, J., Nieminen, T., Ortega, I. K., Wagner, R., Adamov, A., Amorim, A., Bernhammer, A.-K., Bianchi, F., Breitenlechner, M., Brilke, S., Chen, X., Craven, J., Dias, A., Ehrhart, S., Flagan, R. C., Franchin, A., Fuchs, C., Guida, R., Hakala, J., Hoyle, C. R., Jokinen, T., Junninen, H., Kangasluoma, J., Kim, J., Krapf, M., Kürten, A., Laaksonen, A., Lehtipalo, K., Makhmutov, V., Mathot, S., Molteni, U., Onnela, A., Peräkylä, O., Piel, F., Petäjä, T., Praplan, A. P., Pringle, K., Rap, A., Richards, N. A. D., Riipinen, I., Rissanen, M. P., Rondo, L., Sarnela, N., Schobesberger, S., Scott, C. E., Seinfeld, J. H., Sipilä, M., Steiner, G., Stozhkov, Y., Stratmann, F., Tomé, A., Virtanen, A., Vogel, A. L., Wagner, A. C., Wagner, P. E., Weingartner, E., Wimmer, D., Winkler, P. M., Ye, P., Zhang, X., Hansel, A., Dommen, J., Donahue, N. M., Worsnop, D. R., Baltensperger, U., Kulmala, M., Carslaw, K. S., and Curtius, J.: Ion-induced nucleation of pure biogenic particles, Nature, 533, 521, https://doi.org/10.1038/nature17953, 2016.
- Lee, B. H., Lopez-Hilfiker, F. D., Mohr, C., Kurtén, T., Worsnop, D. R., and Thornton, J. A.: An Iodide-Adduct High-Resolution Time-of-Flight Chemical-Ionization Mass Spectrometer: Application to Atmospheric Inorganic and Organic Compounds, Environ. Sci. Technol., 48, 6309–6317, https://doi.org/10.1021/es500362a, 2014.
- Li, Y., Pöschl, U., and Shiraiwa, M.: Molecular corridors and parameterizations of volatility in the chemical evolution of organic aerosols, Atmos. Chem. Phys., 16, 3327–3344, https://doi.org/10.5194/acp-16-3327-2016, 2016.
- Li, H., Almeida, T. G., Luo, Y., Zhao, J., Palm, B. B., Daub, C. D., Huang, W., Mohr, C., Krechmer, J. E., Kurtén, T., and Ehn, M.: Fragmentation inside proton-transfer-reaction-based mass spectrometers limits the detection of ROOR and ROOH peroxides, Atmos. Meas. Tech., 15, 1811–1827, https://doi.org/10.5194/amt-15-1811-2022, 2022.
- Lopez-Hilfiker, F. D., Mohr, C., Ehn, M., Rubach, F., Kleist, E., Wildt, J., Mentel, Th. F., Lutz, A., Hallquist, M., Worsnop, D., and Thornton, J. A.: A novel method for online analysis of gas and particle composition: description and evaluation of a Filter Inlet for Gases and AEROsols (FIGAERO), Atmos. Meas. Tech., 7, 983–1001, https://doi.org/10.5194/amt-7-983-2014, 2014.
- Mellouki, A., Wallington, T. J., and Chen, J.: Atmospheric chemistry of oxygenated volatile organic compounds: impacts on air quality and climate, Chem. Rev., 115, 3984–4014, https://doi.org/10.1021/cr500549n, 2015.
- Mohr, C., Thornton, J. A., Heitto, A., Lopez-Hilfiker, F. D., Lutz, A., Riipinen, I., Hong, J., Donahue, N. M., Hallquist, M., Petäjä, T., Kulmala, M., and Yli-Juuti, T.: Molecular identification of organic vapors driving atmospheric nanoparticle growth, Nat. Commun., 10, 4442, https://doi.org/10.1038/s41467-019-12473-2-2019
- Pankow, J. F. and Asher, W. E.: SIMPOL.1: a simple group contribution method for predicting vapor pressures and enthalpies of vaporization of multifunctional organic compounds, Atmos. Chem. Phys., 8, 2773–2796, https://doi.org/10.5194/acp-8-2773-2008, 2008.

- Pospisilova, V., Lopez-Hilfiker, F. D., Bell, D. M., El Haddad, I., Mohr, C., Huang, W., Heikkinen, L., Xiao, M., Dommen, J., Prevot, A. S. H., Baltensperger, U., and Slowik, J. G.: On the fate of oxygenated organic molecules in atmospheric aerosol particles, Science Advances, 6, eaax8922, https://doi.org/10.1126/sciadv.aax8922, 2020.
- Rissanen, M. P., Mikkilä, J., Iyer, S., and Hakala, J.: Multi-scheme chemical ionization inlet (MION) for fast switching of reagent ion chemistry in atmospheric pressure chemical ionization mass spectrometry (CIMS) applications, Atmos. Meas. Tech., 12, 6635–6646, https://doi.org/10.5194/amt-12-6635-2019, 2019.
- Riva, M., Ehn, M., Li, D., Tomaz, S., Bourgain, F., Perrier, S., and George, C.: CI-Orbitrap: An Analytical Instrument To Study Atmospheric Reactive Organic Species, Anal. Chem., 91, 9419– 9423, https://doi.org/10.1021/acs.analchem.9b02093, 2019a.
- Riva, M., Rantala, P., Krechmer, J. E., Peräkylä, O., Zhang, Y., Heikkinen, L., Garmash, O., Yan, C., Kulmala, M., Worsnop, D., and Ehn, M.: Evaluating the performance of five different chemical ionization techniques for detecting gaseous oxygenated organic species, Atmos. Meas. Tech., 12, 2403–2421, https://doi.org/10.5194/amt-12-2403-2019, 2019b.
- Riva, M., Brüggemann, M., Li, D., Perrier, S., George, C., Herrmann, H., and Berndt, T.: Capability of CI-Orbitrap for Gas-Phase Analysis in Atmospheric Chemistry: A Comparison with the CI-APi-TOF Technique, Anal. Chem., 92, 8142–8150, https://doi.org/10.1021/acs.analchem.0c00111, 2020.
- Schobesberger, S., Junninen, H., Bianchi, F., Lonn, G., Ehn, M., Lehtipalo, K., Dommen, J., Ehrhart, S., Ortega, I. K., Franchin, A., Nieminen, T., Riccobono, F., Hutterli, M., Duplissy, J., Almeida, J., Amorim, A., Breitenlechner, M., Downard, A. J., Dunne, E. M., Flagan, R. C., Kajos, M., Keskinen, H., Kirkby, J., Kupc, A., Kurten, A., Kurten, T., Laaksonen, A., Mathot, S., Onnela, A., Praplan, A. P., Rondo, L., Santos, F. D., Schallhart, S., Schnitzhofer, R., Sipila, M., Tome, A., Tsagkogeorgas, G., Vehkamaki, H., Wimmer, D., Baltensperger, U., Carslaw, K. S., Curtius, J., Hansel, A., Petaja, T., Kulmala, M., Donahue, N. M., and Worsnop, D. R.: Molecular understanding of atmospheric particle formation from sulfuric acid and large oxidized organic molecules, P. Natl. Acad. Sci. USA, 110, 17223–17228, https://doi.org/10.1073/pnas.1306973110, 2013.
- Simon, M., Dada, L., Heinritzi, M., Scholz, W., Stolzenburg, D., Fischer, L., Wagner, A. C., Kürten, A., Rörup, B., He, X.-C., Almeida, J., Baalbaki, R., Baccarini, A., Bauer, P. S., Beck, L., Bergen, A., Bianchi, F., Bräkling, S., Brilke, S., Caudillo, L., Chen, D., Chu, B., Dias, A., Draper, D. C., Duplissy, J., El-Haddad, I., Finkenzeller, H., Frege, C., Gonzalez-Carracedo, L., Gordon, H., Granzin, M., Hakala, J., Hofbauer, V., Hoyle, C. R., Kim, C., Kong, W., Lamkaddam, H., Lee, C. P., Lehtipalo, K., Leiminger, M., Mai, H., Manninen, H. E., Marie, G., Marten, R., Mentler, B., Molteni, U., Nichman, L., Nie, W., Ojdanic, A., Onnela, A., Partoll, E., Petäjä, T., Pfeifer, J., Philippov, M., Quéléver, L. L. J., Ranjithkumar, A., Rissanen, M. P., Schallhart, S., Schobesberger, S., Schuchmann, S., Shen, J., Sipilä, M., Steiner, G., Stozhkov, Y., Tauber, C., Tham, Y. J., Tomé, A. R., Vazquez-Pufleau, M., Vogel, A. L., Wagner, R., Wang, M., Wang, D. S., Wang, Y., Weber, S. K., Wu, Y., Xiao, M., Yan, C., Ye, P., Ye, Q., Zauner-Wieczorek, M., Zhou, X., Baltensperger, U., Dommen, J., Flagan, R. C., Hansel, A., Kulmala, M., Volkamer, R., Winkler, P. M., Worsnop, D. R., Donahue, N.

- M., Kirkby, J., and Curtius, J.: Molecular understanding of new-particle formation from α -pinene between -50 and +25 °C, Atmos. Chem. Phys., 20, 9183–9207, https://doi.org/10.5194/acp-20-9183-2020, 2020.
- Stolzenburg, D., Fischer, L., Vogel, A. L., Heinritzi, M., Schervish, M., Simon, M., Wagner, A. C., Dada, L., Ahonen, L. R., Amorim, A., Baccarini, A., Bauer, P. S., Baumgartner, B., Bergen, A., Bianchi, F., Breitenlechner, M., Brilke, S., Buenrostro Mazon, S., Chen, D., Dias, A., Draper, D. C., Duplissy, J., El Haddad, I., Finkenzeller, H., Frege, C., Fuchs, C., Garmash, O., Gordon, H., He, X., Helm, J., Hofbauer, V., Hoyle, C. R., Kim, C., Kirkby, J., Kontkanen, J., Kürten, A., Lampilahti, J., Lawler, M., Lehtipalo, K., Leiminger, M., Mai, H., Mathot, S., Mentler, B., Molteni, U., Nie, W., Nieminen, T., Nowak, J. B., Ojdanic, A., Onnela, A., Passananti, M., Petäjä, T., Quéléver, L. L. J., Rissanen, M. P., Sarnela, N., Schallhart, S., Tauber, C., Tomé, A., Wagner, R., Wang, M., Weitz, L., Wimmer, D., Xiao, M., Yan, C., Ye, P., Zha, Q., Baltensperger, U., Curtius, J., Dommen, J., Flagan, R. C., Kulmala, M., Smith, J. N., Worsnop, D. R., Hansel, A., Donahue, N. M., and Winkler, P. M.: Rapid growth of organic aerosol nanoparticles over a wide tropospheric temperature range, P. Natl. Acad. Sci. USA, 115, 9122-9127, https://doi.org/10.1073/pnas.1807604115, 2018.
- Surdu, M., Lamkaddam, H., Wang, D. S., Bell, D. M., Xiao, M., Lee, C. P., Li, D., Caudillo, L., Marie, G., Scholz, W., Wang, M., Lopez, B., Piedehierro, A. A., Ataei, F., Baalbaki, R., Bertozzi, B., Bogert, P., Brasseur, Z., Dada, L., Duplissy, J., Finkenzeller, H., He, X.-C., Höhler, K., Korhonen, K., Krechmer, J. E., Lehtipalo, K., Mahfouz, N. G. A., Manninen, H. E., Marten, R., Massabò, D., Mauldin, R., Petäjä, T., Pfeifer, J., Philippov, M., Rörup, B., Simon, M., Shen, J., Umo, N. S., Vogel, F., Weber, S. K., Zauner-Wieczorek, M., Volkamer, R., Saathoff, H., Möhler, O., Kirkby, J., Worsnop, D. R., Kulmala, M., Stratmann, F., Hansel, A., Curtius, J., Welti, A., Riva, M., Donahue, N. M., Baltensperger, U., and El Haddad, I.: Molecular Understanding of the Enhancement in Organic Aerosol Mass at High Relative Humidity, Environ. Sci. Technol., 57, 2297–2309, https://doi.org/10.1021/acs.est.2c04587, 2023.
- Viggiano, A. A., Seeley, J. V., Mundis, P. L., Williamson, J. S., and Morris, R. A.: Rate Constants for the Reactions of $XO_3^-(H_2O)_n$ (X = C, HC, and N) and $NO_3^-(HNO_3)$ n with H_2SO_4 : Implications for Atmospheric Detection of H_2SO_4 , J. Phys. Chem. A, 101, 8275–8278, https://doi.org/10.1021/jp971768h, 1997.
- Wang, M., Kong, W., Marten, R., He, X.-C., Chen, D., Pfeifer, J., Heitto, A., Kontkanen, J., Dada, L., Kürten, A., Yli-Juuti, T., Manninen, H. E., Amanatidis, S., Amorim, A., Baalbaki, R., Baccarini, A., Bell, D. M., Bertozzi, B., Bräkling, S., Brilke, S., Murillo, L. C., Chiu, R., Chu, B., De Menezes, L.-P., Duplissy, J., Finkenzeller, H., Carracedo, L. G., Granzin, M., Guida, R., Hansel, A., Hofbauer, V., Krechmer, J., Lehtipalo, K., Lamkaddam, H., Lampimäki, M., Lee, C. P., Makhmutov, V., Marie, G., Mathot, S., Mauldin, R. L., Mentler, B., Müller, T., Onnela, A., Partoll, E., Petäjä, T., Philippov, M., Pospisilova, V., Ranjithkumar, A., Rissanen, M., Rörup, B., Scholz, W., Shen, J., Simon, M., Sipilä, M., Steiner, G., Stolzenburg, D., Tham, Y. J., Tomé, A., Wagner, A. C., Wang, D. S., Wang, Y., Weber, S. K., Winkler, P. M., Wlasits, P. J., Wu, Y., Xiao, M., Ye, Q., Zauner-Wieczorek, M., Zhou, X., Volkamer, R., Riipinen, I., Dommen, J., Curtius, J., Baltensperger, U., Kulmala, M., Worsnop, D. R.,

Kirkby, J., Seinfeld, J. H., El-Haddad, I., Flagan, R. C., and Donahue, N. M.: Rapid growth of new atmospheric particles by nitric acid and ammonia condensation, Nature, 581, 184–189, https://doi.org/10.1038/s41586-020-2270-4, 2020.